Assessing the Feasibility of Brain Imaging with Ultrasound Tomography: *In-Silico* and *In-Vitro* Evaluation

Melanie Singh*, Rehman Ali*, Trevor Mitcham*, Israel Owolabi*, Victoria Nketia*, Alex Klaben*, Nebojsa Duric*

*University of [1]Rochester, Department of Imaging Sciences, Rochester, NY, USA.

Abstract

Ultrasound Tomography (UST) provides a non-invasive way to reconstruct high-resolution images of tissue properties. When there is a high contrast between tissue properties, limited low-frequency signal content makes it difficult to apply UST to brain imaging, especially when high-impedance structures like bone are present. This study used both *in-silico* and *in-vitro* experiments to assess the viability of UST for brain imaging. A frequency-domain full waveform inversion (FWI) algorithm was used for image reconstructions. The impact of reconstruction parameters on image quality was methodically investigated. We validate our simulation techniques through comparison with experimental data and provide useful guidance for enhancing UST-based brain imaging in clinical settings. Results show that frequencies as low as 50 kHz may be needed to mitigate cycle skipping artifacts and using smaller iterative step sizes further stabilized the reconstructions against cycle skipping.

1. Introduction

Traumatic and nontraumatic brain injuries are as unique and complex as the individual brain. As such, patient outcomes exhibit large variability, especially when such injuries involve vascular damage. Each minute of oxygenated blood deprivation to an area of the brain results in the death of millions of neurons [1]. The gold standard for imaging brain hemorrhages is CT due to its superior sensitivity to intracranial blood compared to MRI [2]. Both CT and MRI have high energy demands and machines hold high operating and upfront costs, thus confining both modalities to larger medical centers. This negatively impacts patients in remote and underserved areas. Time is vital in brain injuries, delays introduced by travel times to the medical centers compounded with interfacility transfers for imaging increases mortality. The largest number of fatalities among mild to moderate TBI patients is seen between triage and diagnostic imaging [3]. The Glasgow Coma Scale is initially used to evaluate patients with brain injuries but overlooks the uniqueness of each injury [4]. Scores are used to prioritize imaging patients based on perceived need. The lack of dedicated imaging machinery for brain injuries introduces delays in diagnosis leading to a higher mortality rate. Considering that the leading cause of death and disability is traumatic brain injury in children and adolescents and the fifth leading cause of death and leading cause of disability is stroke in adults,

*Melanie Singh: melaniesingh@rochester.edu

Medical Imaging 2026: Ultrasonic Imaging and Tomography, edited by Christian Boehm, Mohammad Mehrmohammadi, Shawn Liangzhong Xiang, Proc. of SPIE Vol. 13931, 1393106 · 2026 Published by SPIE
1605-7422 · doi: 10.1117/12.3086112

there is a clear need for a safe, rapid, efficient, and accessible imaging modality capable of detecting brain bleeds [5, 6].

Ultrasound imaging is one of the most widely employed imaging technologies, serving as a key diagnostic tool in various medical fields and is the gold standard in obstetric imaging. Despite its widespread adoption, there are still no ultrasound imaging systems capable of producing diagnostic quality images of the brain [7]. However, the proposed method of using transmitted ultrasound rays for derivation of tissue properties has evolved extensively. Recent technological advancements have further facilitated progress in ultrasound imaging which allowed for higher resolution images and enabled the use of more robust reconstruction techniques. Therefore, it is unsurprising to see new modalities emerge such as ultrasound tomography; a method which uses both transmitted and reflected signals to generate images of tissue properties. Currently, there is an FDA approved ultrasound tomographic imaging system used for adjunctive breast cancer screening [8].

Ultrasound imaging is used for more superficial clinical applications, where bone is not a concern. The skull poses its own distinct challenges to ultrasound. Comprised of one layer of spongy cancellous bone encased by dense cortical bone, the skull significantly reflects, refracts, and attenuates ultrasound signals at conventional imaging frequencies. Attenuation primarily affects the signal to noise ratio, reducing the quality of the signal. However, this is frequency dependent, therefore mediated through use of low frequency ultrasound [9].

This research utilizes *in-silico* and *in-vitro* experiments to explore the potential applications of UST techniques for diagnosis of brain injury. This method utilizes a full waveform inversion algorithm to reconstruct sound speed images. Unlike conventional reflection pulse-echo ultrasound, UST models the full diffractive effects of acoustic propagation. A full waveform inversion algorithm uses the mismatch between the measured signal and a simulated signal to reconstruct images of material properties [10]. These images are susceptible to artifacts induced when there is high contrast between material properties. Nevertheless, previous experiments show that there is some potential for this technique in through-skull brain imaging. Guasch et al found an improvement in brain images after implementing their adaptive waveform inversion technique. [11] The use of lower frequencies can mitigate these phenomena, as we show below. We present and discuss results obtained from the optimization of image reconstruction parameters.

2. Methods

2.1 Phantom Development

Two phantoms, *in-vitro* and *in-silico,* were used to evaluate the potential of ultrasound tomography for brain imaging and to test optimal experimental parameters. Additional testing was performed to establish the empirical validity of the simulated data with respect to the experimental data. Phantom

design aims to evaluate the abilities of ultrasound tomography to penetrate the skull and detect inclusions within the skull for brain imaging applications (Figure 1).

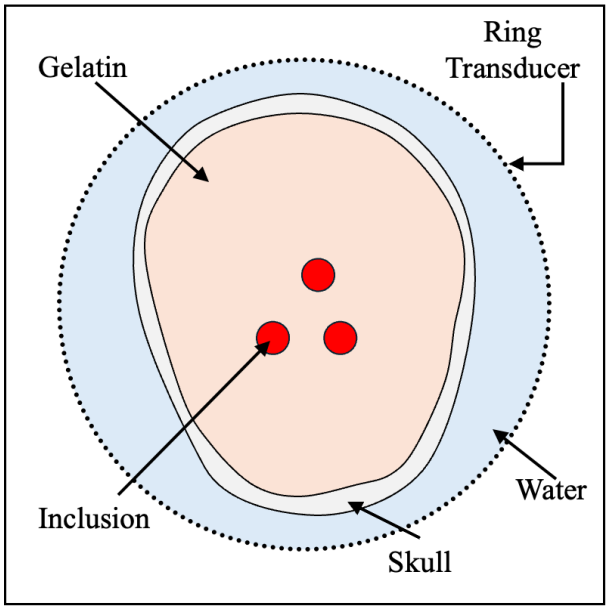

Figure 1: Schematic of phantom used in *in-vitro* and *in-silico* experiments.

The *in-vitro* phantom is composed of a gelatin phantom with high impedance targets encased in a human skull. The skull is cut directly above the frontal sinus to remove the calvaria while avoiding any air-filled cavities. The experimental phantom consists of parietal bone with the upper sections of the frontal and occipital bones. This yielded a bowl shape that the gelatin phantom was cast. A mixture of 8% gelatin (Sigma-Aldrich, Inc., St. Louis, MO) and 0.5% silica powder (US Silica, Katy, TX) was directly poured into the calvaria to create the background (~1520 m/s). Three 1-cm diameter cylindrical molds were immediately placed into the uncured gelatin. Once cured, the molds were removed and these spaces were backfilled with an 8% gelatin and 20% alcohol mixture to produce the high sound speed inclusions (~1600 m/s).

The *in-silico* phantom was derived from a head CT image. The head CT was obtained from an open-source dataset; a scan of a patient with no injuries was selected for the phantom [12]. Thresholding was used to define a rough skull segmentation. A piecewise function was used to map the Hounsfield units from the CT image to sound speed (m/s) and density (kg/m^3) such that the average speed of sound and density of the skull was 2410 m/s and 1803 kg/m^{3,} respectively [13, 14]. The area inside the skull was set to 1520 m/s and 1050 kg/m^3; these values closely resemble that of our gelatin phantom while maintaining relevance to soft brain tissue [15]. Inclusions were added in accordance with the schematic shown in Figure 1. Three points around the center of the skull were selected and used to position three 1.5-cm diameter inclusions. The sound speed and density of the inclusions are set to 1565m/s and 1060kg/m^3, respectively. These values maintain the native contrast in sound

speed parameters seen between blood and brain tissue. Much like the clinical UST system, water was used as a coupling agent. This is reflected in the background of the phantom (Figure 2).

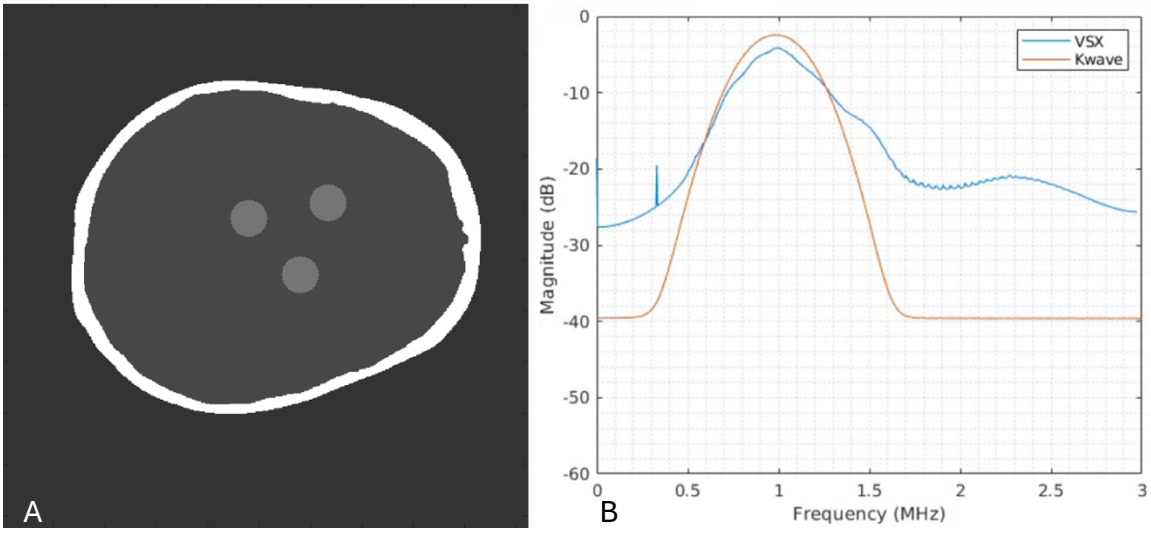

Figure 2: Numerical phantom used for *in-silico* experiments (A). The skull is derived from a CT image [12]. The average speed of sound is 2410 m/s in the skull, 1520 m/s in the gelatin, 1565 m/s in the inclusions, and 1500 m/s for the background. The spectral response of the transducer used in the *in vitro* (blue) and the simulated transducer used in the *in silico* (orange) experiments is shown (B). Both spectra have adequate signal content between 300 kHz and 1.7 MHz.

2.2 In-Vitro Experiments

In-vitro experiments were conducted using a Verasonics Vantage NXT (Verasonics Inc., Kirkland, WA) with a 256-element ring array (TransducerWorks, LLC, Centre Hall, PA; 1.5-MHz center frequency). A transmit frequency of 1MHz was used. This experimental system reflects the parameters of current clinically available UST systems, offering comparable bandwidth and resolution with a slightly lower center frequency. This change makes the ring better suited for brain imaging because low frequency waves are less attenuated by the skull. Water was used as a coupling agent. The resulting spectrum indicates that the lowest frequency available for reconstruction was around 300 kHz. The SNR of the measured signal lies approximately 20 dB above the noise floor, indicating that this method can generate ultrasound pulses which remain detectable following transmission through the skull. (Figure 2)

2.3 K-Wave Simulations

The MATLAB toolbox K-wave was used to simulate ultrasound propagation through the medium [16]. The transducer geometry mimics the clinical system with 512 elements arranged in a ring formation with a 22-cm diameter. A signal of 1 MHz is used for imaging with 50% bandwidth; this frequency can be acquired by current clinical systems and experimental systems. Each element

operates as both a transmitter and receiver. Ultrasound propagation was simulated such that each transducer would fire independently and the signal then measured on all other transducers. The resulting RF data was then processed, and white Gaussian noise was added. This produced a signal that closely resembles the bandwidth of the signal obtained from the *in-vitro* experiments (Figure 2). For other tests, the noise level is varied to reflect optimal parameters.

2.4 Image Reconstruction

A frequency domain full waveform inversion algorithm was used to perform image reconstruction. At each iteration, the 2D Helmholtz equation was solved using finite difference methods with respect to frequency, source, and speed of sound [17, 18]. The error between the calculated and experimental waveforms was used to guide updates to the sound speed map. As the algorithm progresses, the residual between the calculated and experimental waveform lessens resulting in a high-resolution image of tissue sound speed.

Considering that both the *in-silico* and *in vitro* datasets have limited signal below 300 kHz, additional techniques are required to ensure model stability and convergence. In this case, we employed frequency differencing full waveform inversion (FD-FWI) to simulate signals below 300 kHz by taking the ratios of two different signals to generate a synthetic low frequency [19]. While this method is effective in reducing cycle skipping, it is imperative to avoid over fitting the model in as these signals are synthetically generated. Initial reconstructions use a frequency range of 50 kHz to 750 kHz, where frequency differencing is used to acquire frequencies from 50 kHz to 300 kHz, the experimental signal is used for the remaining frequencies. The frequency step is varied between reconstructions, this parameter ranges from 5 kHz to 50 kHz.

3. Results

3.1 In-vitro Results

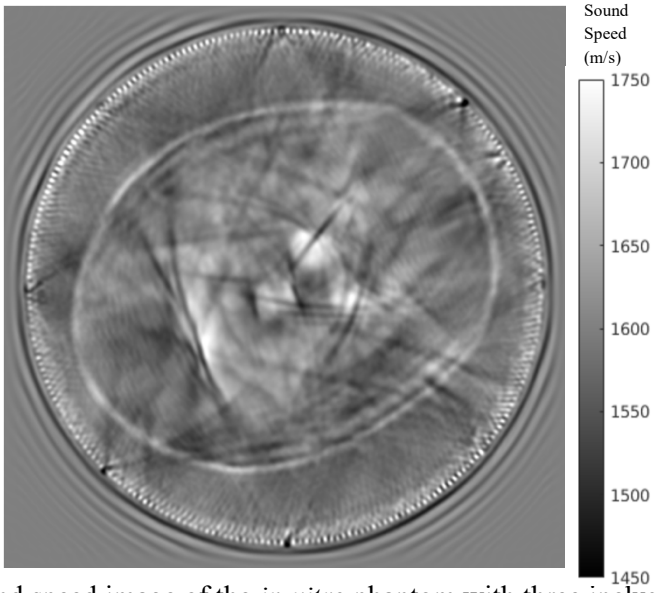

Figure 3: Reconstructed sound speed image of the *in-vitro* phantom with three inclusions despite cycle skipping artifacts. Reconstruction utilizes frequencies from 350 kHz to 750 kHz with a 50 kHz step size.

Current experimental UST hardware can image inclusions within the skull as shown in Figure 3. Cycle skipping has a heavy presence in the image. The skull reconstructs as alternating regions of high and low sound speed. The high sound speed regions of the skull reconstruct to a maximum value of 1958 m/s. Concentric ring artifacts appear in the center of the skull. This oscillatory artifact generates blur seen at the boundaries of the individual inclusions.

3.2 In-silico Results

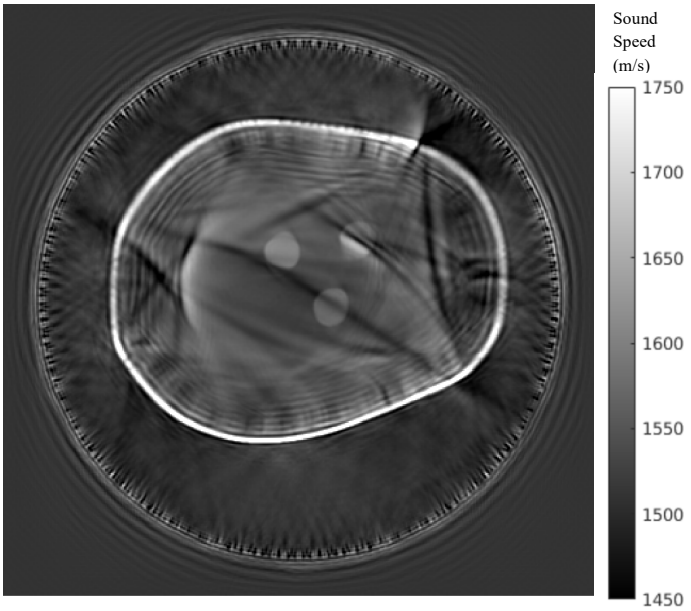

Figure 4: Reconstructed sound speed image of the *in-silico* phantom showing all three inclusions despite partial obfuscation from cycle skipping artifacts. Reconstruction utilizes frequencies from 350kHz to 750 kHz with a 5 kHz step size.

In-silico experiments using matched hardware parameters are also able to visualize all three inclusions (Figure 4). Cycle skipping artifacts manifest as the streaking regions of low sound speed which affect the inclusions. The boundaries of the inclusions do not appear as perfect circles; shape distortions are present. The skull reconstructs as concentric rings of high and low sound speed, with a maximum sound speed of 1889.1 m/s. The RMSE between the reconstructed image and the ground truth is 245.95 m/s.

3.3 Frequency Differencing in-silico Results

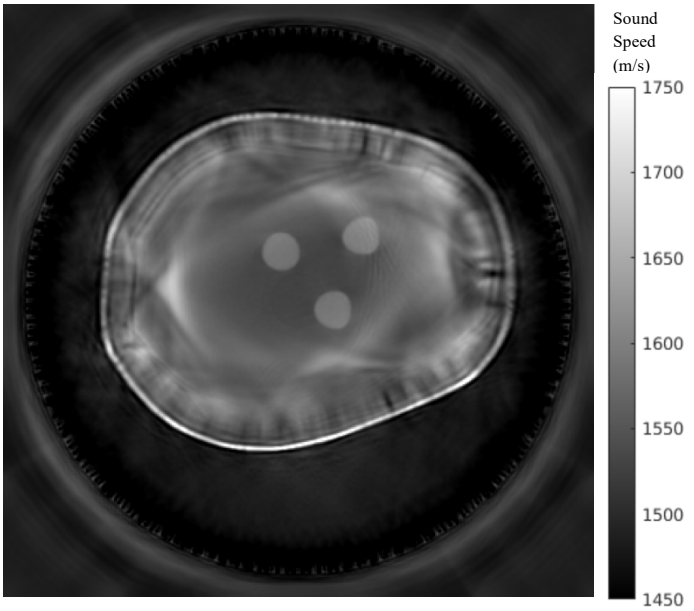

Figure 5: Reconstructed sound speed image of the *in-silico* phantom using FD-FWI to mediate cycle skipping with clear visualization of all three inclusions. This image utilizes frequency differencing to synthesize frequencies from 50 kHz to 300 kHz with a 10 kHz step size. A 5 kHz step size is used to reconstruct frequencies from 350 kHz to 750 kHz. The update is damped such that only 10% of each update is performed.

Frequency differencing significantly improved image appearance, mediating severe cycle skipping artifacts. Inclusions are easily visualized, though there are some minor deformations in the reconstructed shape. Most artifacts are concentrated at the skull brain boundary. The region of the brain adjacent to the frontal bone exhibits multiple regions of low sound speed. The skull still reconstructs as regions of high and low sound speed. While the concentric ring shape is present, artifacts perpendicular to the skull appear worse. The highest sound speed in this region is 1770 m/s. The RMSE is 276.39 m/s.

3.4 Low Frequency in-silico Results

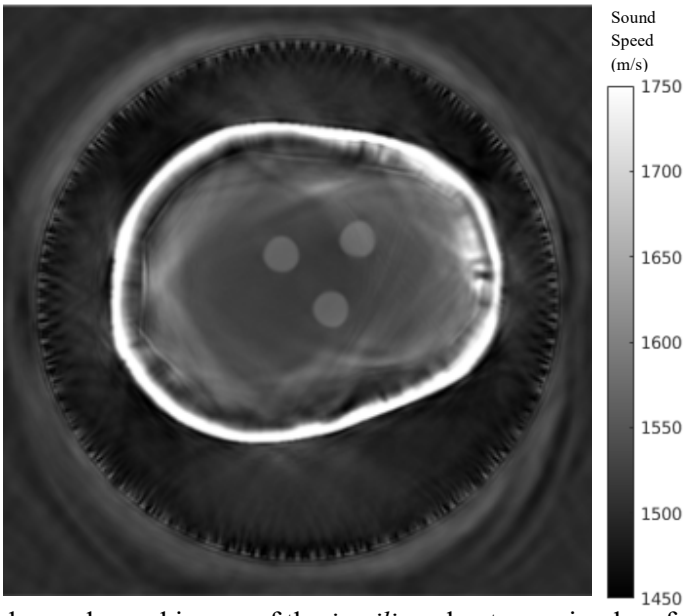

Figure 6: Reconstructed sound speed image of the *in-silico* phantom using low frequency FWI from 50 kHz to 750 kHz with a 5 kHz step size. This image clearly depicts all three inclusions within a uniform skull boundary. The update is damped such that only 10% of each update is performed.

The use of low frequency signal content significantly improved visualization of the skull. Most skull artifacts were concentrated in the frontal bone. The maximum skull sound speed was found to be 2395.9 m/s, which is comparable to mean sound speed of the skull in the ground truth. Adjacent to the skull there is a region of low sound speed with some artifacts. All three inclusions are reconstructed as near perfect circles indicating the potential of this technique to clearly visualize inclusions in the skull. The RMSE is reduced to 160.6 m/s.

4. Discussion

This work shows that UST can transmit and receive signals through the skull in numerical simulations and laboratory conditions. Across all imaging scenarios, three inclusions are consistently visualized within the skull, indicating that FWI can reconstruct features within the skull. This study also showed that cycle skipping could be mitigated. When using data consistent with current clinical technology, severe artifacts were present. As low frequency signal content was introduced, artifacts were minimized. Additionally, we have shown that many of the artifacts present during *in-vitro* experiments persist in the *in-silico* dataset. This indicates that methods used for *in-silico* experiments can emulate more complex wave phenomena and are comparable to benchtop conditions despite the high contrast medium.

All three inclusions are visualized across all four reconstruction scenarios, showing that UST can overcome challenges posed by the high impedance skull. Figure 3 shows much blurring and some

smearing of the inclusions. Cycle skipping artifacts also degrade the image quality. Both cycle skipping and blur persist into Figure 4. The boundaries tighten and the inclusions look clear in Figures 5 and 6. Severe cycle skipping artifacts are eliminated when reconstructions use a starting frequency of 50kHz. Cycle skipping occurs when the error between the measured and modelled data is greater than half a wavelength. Lower starting frequencies effectively increase the error window such that convergence is possible despite initial mismatch.

The skull was the main challenge when applying ultrasound tomography to brain imaging. Figures 3 and 4 show the resulting sound speed images from the matched *in-vitro* and *in-silico* experiments. Interestingly, the same skull artifact is present in both reconstructions. The skull appears as a faint disk of uniform thickness. However, the skull in both the calvarium and numerical dataset had varying thickness. Adjacent to the skull is an overestimation in sound speed. This misrepresentation can be used to explain the underestimation in the skull. Inaccurate modeling of high contrast structures results in numerous artifacts and as the algorithm continues to fit the modelled waveform to the measured data, these artifacts cannot be corrected and are instead propagated obscuring adjacent features. This shows that simulated data is susceptible to the same application-specific interactions as the *in-vitro* data.

Considering that high frequency signals are heavily attenuated by the skull, the use of lower frequency signals could alleviate some of the error. One concern is that frequency differenced data may carry over high frequency artifacts to derived low frequency data. Figures 5 and 6 show that when a starting frequency of 50 kHz is used artifacts are less intense and cycle skipping is minimized. When low frequency signals are measurable against the noise, a more accurate skull is formed, with varying thickness represented. Frequency differencing can produce signals which overcome artifacts due to cycle skipping but lack the information to produce a geometrically accurate skull.

5. Conclusions

The *in-silico* experiments were shown to be consistent with the *in-vitro* experiments. The *in-silico* experiments were able to reproduce the artifacts seen in the *in-vitro* experiments when low frequencies were not present. Extension of the *in-silico* experiments to lower frequencies demonstrated a clear reduction in cycle skipping artifacts. In totality, this work shows that frequencies as low as 50 kHz may be needed to perform transcranial whole-brain imaging with UST.

References

1. Saver, J.L., *Time is brain—quantified.* Stroke, 2006. **37**(1): p. 263-266.
2. Jain, A., A. Malhotra, and S. Payabvash, *Imaging of spontaneous intracerebral hemorrhage.* Neuroimaging Clinics, 2021. **31**(2): p. 193-203.

3. Vaca, S.D., et al., *Temporal delays along the neurosurgical care continuum for traumatic brain injury patients at a tertiary care hospital in Kampala, Uganda.* Neurosurgery, 2019. **84**(1): p. 95-103.
4. Matis, G. and T. Birbilis, *The Glasgow Coma Scale–a brief review Past, present, future.* Acta Neurol Belg, 2008. **108**(3): p. 75-89.
5. Association, A.S.-L.-H. *Pediatric Traumatic Brain Injury*. [cited 2024.
6. Martin, S.S., et al., *2024 heart disease and stroke statistics: a report of US and global data from the American Heart Association.* Circulation, 2024. **149**(8): p. e347-e913.
7. Quan, Y. and L. Huang. *Sound-speed tomography using first-arrival transmission ultrasound for a ring array*. in *Medical Imaging 2007: Ultrasonic Imaging and Signal Processing*. 2007. SPIE.
8. Duric, N., P. Littrup, and C. Kuzmiak, *Breast ultrasound tomography.* Breast Imaging, 2018. **6**.
9. Pichardo, S., V.W. Sin, and K. Hynynen, *Multi-frequency characterization of the speed of sound and attenuation coefficient for longitudinal transmission of freshly excised human skulls.* Phys Med Biol, 2011. **56**(1): p. 219-50.
10. Virieux, J. and S. Operto, *An overview of full-waveform inversion in exploration geophysics.* Geophysics, 2009. **74**(6): p. WCC1-WCC26.
11. Guasch, L., et al., *Full-waveform inversion imaging of the human brain.* NPJ digital medicine, 2020. **3**(1): p. 28.
12. Hssayeni, M.D., et al., *Intracranial hemorrhage segmentation using a deep convolutional model.* Data, 2020. **5**(1): p. 14.
13. White, P.J., G.T. Clement, and K. Hynynen, *Longitudinal and shear mode ultrasound propagation in human skull bone.* Ultrasound in medicine & biology, 2006. **32**(7): p. 1085-1096.
14. Peterson, J. and P.C. Dechow, *Material properties of the human cranial vault and zygoma.* The Anatomical Record Part A: Discoveries in Molecular, Cellular, and Evolutionary Biology: An Official Publication of the American Association of Anatomists, 2003. **274**(1): p. 785-797.
15. Duck, F., *Physical properties of tissues: a comprehensive reference book*. 2013: Academic press.
16. Treeby, B.E. and B.T. Cox, *k-Wave: MATLAB toolbox for the simulation and reconstruction of photoacoustic wave fields.* Journal of biomedical optics, 2010. **15**(2): p. 021314-021314-12.
17. Ali, R., et al., *2-D slicewise waveform inversion of sound speed and acoustic attenuation for ring array ultrasound tomography based on a block LU solver.* IEEE transactions on medical imaging, 2024. **43**(8): p. 2988-3000.
18. Chen, Z., et al., *An optimal 9-point finite difference scheme for the Helmholtz equation with Pml.* International Journal of Numerical Analysis & Modeling, 2013. **10**(2).
19. Ali, R., et al., *Frequency-differencing strategy to kickstart full-waveform inversion without cycle skipping.* JASA Express Letters, 2025. **5**(1).